Mobility Analysis of a Tumbling and Hopping Rover with An Inner Actuator and Several Elastic Spikes in Microgravity

MOBILITY ANALYSIS OF A TUMBLING AND HOPPING ROVER WITH AN INNER ACTUATOR AND SEVERAL ELASTIC SPIKES IN MICROGRAVITY

*Keita Kobashi[1], Kenji Nagaoka[2], Kazuya Yoshida[1]

[1] *Department of Aerospace Engineering, Tohoku University, Aoba 6-6-01, Aramaki, Aoba-ku, Sendai, Japan, E-mail: {kobashi, yoshida}@astro.mech.tohoku.ac.jp*

[2] *Department of Mechanical and Control Engineering, Kyushu Institute of Technology, Sensuicho 1-1, Tobata-ku, Kitakyushu, Japan, E-mail: nagaoka.kenji572@mail.kyutech.jp*

ABSTRACT

This paper presents the analyses of the tumbling and hopping mobility of a novel moving mechanism on small celestial bodies in microgravity. The robot consists of an inner motor with a flywheel and eight elastic spikes connected to the perimeter of the robot. The tumbling and hopping motion of the robot can be switched by controlling the torque of the motor. Hence, the robot can traverse a large region with high moving accuracy. In this paper, we conduct several numerical simulations to analyze the characteristics of the mobility by assigning various values of elastic and damping coefficient of spikes, and the torque of the motor. The results are useful to construct the feasible motion planning for real missions.

1 INTRODUCTION

In recent years, asteroid exploration has attracted scientists due to the wealth of clues which reveal the origin of our solar system asteroids are expected to have. For the detailed investigation of asteroids, utilization of locomotive robots is an effective exploration method. The gravitational acceleration of asteroid surfaces is estimated to be between 1.0×10^{-5} m/s^2 and 1.0×10^{-2} m/s^2. Several locomotion mechanisms have been invented so far, however, due to the microgravity environment, the candidates of the feasible mechanisms for locomotion on asteroid surfaces are limited. For instance, wheeled locomotion, which is the most prevailing mechanism for space exploration, is less likely to achieve sufficient locomotion [1] because this mechanism utilizes the frictional forces between a robot and the surfaces and the magnitude of the frictional forces depends on the acceleration of gravity. Moreover, robots adopting the wheeled mobility are prone to experience unintentional detachment from the surfaces [2].

To cope with the technical challenges involved in wheeled mobility, hopping [3], [4], [5], ciliary vibration [6], and limbed locomotion [7] were considered. To begin with, we mention the hopping mobility.

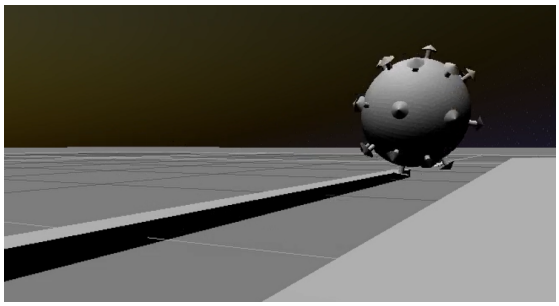

Figure 1 : 3D image of the proposed system

Inner-actuated hopping mobility is a promising method to move on asteroid surfaces because it realizes a simple mechanical system and the capability to traverse uneven surfaces. This mobility is induced by internal impulsive forces derived from motors with flywheels [8], the deformation of a bimetal exposed to a temperature gradient [9], and the elastic energy stored in internal buckling springs [10]. However, robots utilizing this mobility rebound repeatedly after hopping. For this reason, it is difficult to achieve a desired initial velocity and realize the soft landing.

Ciliary vibration locomotion generated by an internal motor with eccentric masses [11] also has a simple mechanical system and this mobility enables robots to move accurately. Although this mechanism enables accurate locomotion, the motion is limited to crawling and consequently has great difficulty traversing uneven surfaces.

Limbed locomotion [7] demonstrates its high capability to traverse uneven surfaces by grasping boulders. However, to realize this locomotion, robots require several legs with some joints and this leads to increasing the cost for development and the failure risks for operation. Moreover, to utilize such complex limbed systems, intricate gait control is required.

The tumbling locomotion displayed in Fig. 1 ex-

hibits a simple mechanical system with several elastic spikes through linear springs and dampers and an inner actuator. This locomotion is able to traverse uneven surfaces by utilizing the elastic damping forces derived from the deformation of its spikes and this contributes to increasing the predictability of the moving direction. Moreover, this simple mechanical system also realizes hopping mobility by changing the magnitude of the motor's torque. Therefore, by applying the hopping mobility when obstacles are too large to traverse by the tumbling motion, the robot can move across a vast scope of asteroid surfaces with high moving accuracy. For these reasons, analyses of the characteristics of tumbling and hopping motion are quite important for the application of this mechanical system to real exploration missions.

In this paper, we evaluate the characteristics of the tumbling and hopping motion by 2-dimensional numerical simulations. In chapter 2, the locomotion mechanism and the dynamics model of the robot is mentioned. In chapter 3, the capability of the proposed system to realize moving modes is addressed. In chapter 4, the analyses of hopping mobility are conducted and the characteristics of the hopping mobility is discussed. In chapter 5, the analyses of tumbling mobility are conducted and the characteristics of the tumbling mobility is discussed. The dynamics model mentioned and utilized in this study has been validated by my previous work [12].

2 LOCOMOTION MECHANISM AND DYNAMICS MODELING

2.1 Locomotion Mechanism

In this section, we address the locomotion mechanism of the tumbling motion. Fig. 2 (a) displays the 2-dimensional schematic figure of the proposed mechanical system. As shown in Fig. 2 (a), the robot has an inner motor with a flywheel at the geometric center and eight elastic spikes around the perimeter of its body. When the internal motor starts rotating, the reaction torque is induced and this leads the robot to rotate. After rotating, the robot utilizes the elastic and damping forces derived from the deformation of the spikes to propel and to continue its tumbling motion. The feasibility of this mechanism has been demonstrated by physical experiments [12].

2.2 Dynamics Modeling

In this study, we consider the 2-dimensional dynamics of the proposed mechanical system. Fig. 3 displays the forces acting on the robot. From Fig. 3, the equations of motion can be described as follows:

$$m\frac{d^2x}{dt^2} = \sum_{i=1}^{n} f_i \tag{1}$$

$$m\frac{d^2y}{dt^2} = -mg + \sum_{i=1}^{n} N_i \tag{2}$$

$$I\frac{d^2\theta}{dt^2} = \sum_{i=1}^{n} N_i r_i \cos\phi_i - \sum_{i=1}^{n} f_i r_i \sin\phi_i + T_M \tag{3}$$

The dynamical interaction between the body and the spikes is modeled by elastic and damping forces since the spikes are connected through linear springs and dampers.

$$N_i = \frac{T_M}{r_i}\cos\phi_i + F_{K_i}\sin\phi_i \tag{4}$$

Table 1 : Variables in Equations

Variables	Name
m	Total mass of the robot
x	Horizontal position of the robot
y	Vertical position of the robot
n	Number of spikes in contact with the ground
i	Index of spikes
f_i	Frictional forces acting on the ith spike
g	Acceleration of gravity
N_i	Normal forces acting on the ith spike
I	Moment of inertia of the robot
θ	Attitude of the robot
r_i	Rotational radius between the body and the spike
ϕ_i	Angle between the ith spike and the ground
T_M	Centrifugal torque of the motor
v_{x_i}	Horizontal portion of translational velocity of the ith spike
μ	Static friction coefficient
μ_d	Dynamic friction coefficient
F_{K_i}	Elastic and damping force of the ith spike
K	Elastic coefficient of a linear spring
h_0	Initial length of a linear spring
h	Length of a linear spring
D	Damping coefficient of a damper
θ_{hop}	Hop angle of the robot
$v_{x_{\mathrm{hop}}}$	Horizontal portion of hop velocity of the robot
$v_{y_{\mathrm{hop}}}$	Vertical portion of hop velocity of the robot
F	Sum of the reaction forces
Δt	Period of maintaining contact with the ground

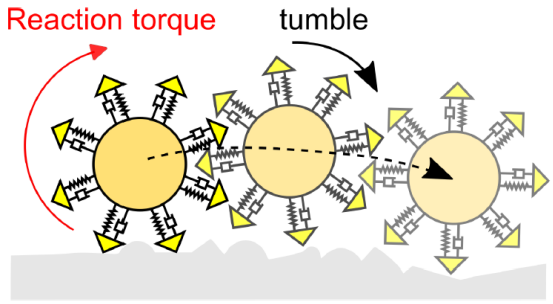

(a) Mechanical system and moving mechanism

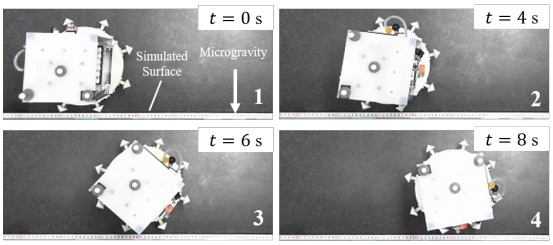

(b) Validation of the feasibility

Figure 2 : Notion and feasibiity of the mechanical system and the moving mechanism

$$f_i = \begin{cases} \dfrac{T_M}{r_i}\sin\phi_i - F_{K_i}\cos\phi_i & \text{(Static Friction)} \\ -\mathrm{sgn}(v_{x_i})\mu N_i & \text{(Maximum Static Friction)} \\ -\mathrm{sgn}(v_{x_i})\mu_d N_i & \text{(Dynamic Friction)} \end{cases} \tag{5}$$

$$F_{K_i} = K(h_0 - h) - D\frac{dh}{dt} \tag{6}$$

Besides, in the context of evaluating the hopping mobility, the hop angle θ_{hop} is an important parameter. In this paper, we define θ_{hop} as the following equation.

$$\theta_{\mathrm{hop}} = \tan^{-1}\frac{v_{x_{\mathrm{hop}}}}{v_{y_{\mathrm{hop}}}} \tag{7}$$

As described in Eq. 7, the hop angle is the ratio of the horizontal and vertical portion of the translational velocity of the robot at the time of detaching from the surface. We define that the initial translational velocity at the time of detaching from the surface is hop velocity.

Here, the variables used in these equations are listed in Tab. 1.

3 MOVING MODES

In this section, we mention the three moving modes with their definitions.

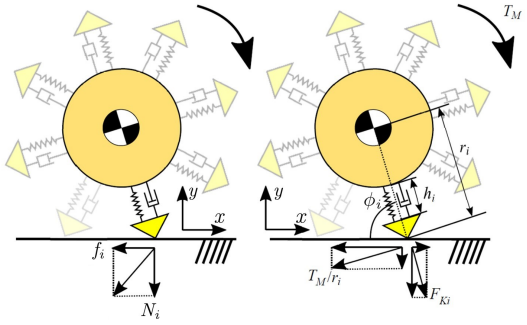

Figure 3 : Dynamics model

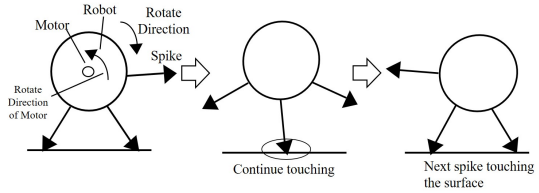

(a) Tumbling

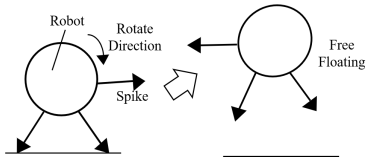

(b) Hopping

Figure 4 : Definition of motion

1. Tumbling: As shown in Fig, 4 (a), the spikes of the robot contact the ground, sequentially. Periods of no contact with the ground are possible; however, less than a revolution in the air is required.

2. Hopping: As shown in Fig. 4 (b), contact is not maintained with the ground. The spikes of the robot are not required to contact the ground sequentially. A single revolution or more is necessary while floating in the air.

An example of a motion sequence of tumbling and hopping is shown in Fig. 5. We apply the torque to the robot for 0.3 seconds. Besides, the time profiles of the position of the geometric center of the robot while tumbling and hopping are shown in Fig. 6. Fig. 6 indicates the capability that the proposed mechanical system realizes the tumbling and hopping motion in a microgravity environment by changing the magnitude of the torque. If the acceleration of gravity is $10^{-6}\mathrm{m/s^2}$ or less, the robot tends to realize the hopping motion. The reason is that the pushing force of the robot becomes small in the case of desiring the tumbling locomotion and the center of the vibration

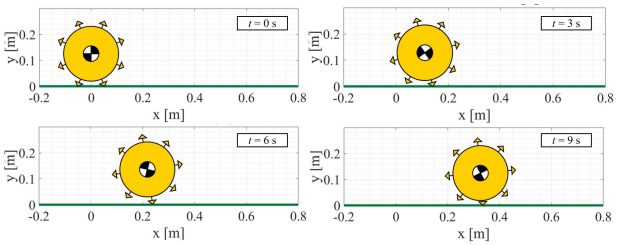

(a) Tumbling

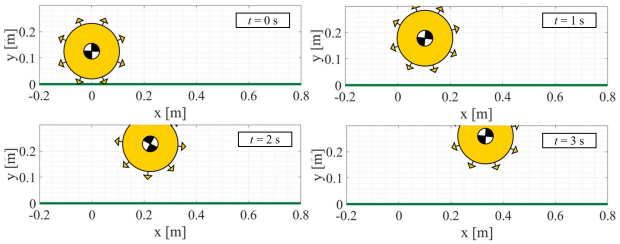

(b) Hopping

Figure 5 : An example of a motion sequence of tumbling and hopping

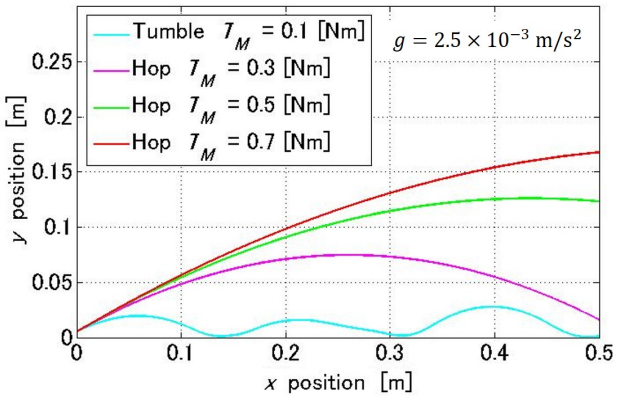

Figure 6 : Time profile of the postion of the geometric center while tumbling and hopping

of a spike in contact with the ground shifts toward the body of the robot and the length of the spike tends to exceed its natural length. Thus, the spike can easily detach from the ground and finally, the robot starts floating. For these reasons, the hopping motion is likely to emerge in such environments.

4 SIMULATION ANALYSES OF HOPPING MOBILITY

We discuss the hopping motion of the proposed mechanical system. Several numerical analyses are conducted to evaluate the characteristics of the hopping motion. At first, the parameter of the robot is listed in Tab. 2

In this section, all simulations are executed in $g = 2.5 \times 10^{-3}$ m/s^2 environment.

4.1 Analyses of Hop Angle

In this section, we assess the hopping mobility of the robot by focusing on the hop angle mentioned in Eq. 7. To begin with, we assign several elastic and coefficient of a linear spring K and a damper D, and observe how the hopping behavior changes. The parameters used in this simulation are listed in Tab. 3.

In this case, the hop angle does not change significantly. In the case of the hopping motion, the robot receives a large torque, hence, the period in contact with the ground is quite short. For this reason, the elastic and damping forces do not significantly affect the impulse the robot receives before the detachment from the ground. Moreover, we consider enlarging

Table 2 : Parameters of the robot

Variables [Unit]	Value
m [kg]	4.45
g [m/s^2]	2.5×10^{-3}
I [kgm^2]	0.0154
μ	2.25
μ_d	1.8
h_0 [m]	0.015
r_{body} [m]	0.10607
l_{spike} [m]	0.015

Table 3 : Simulation conditions for analyzing hop angle against K and D

Variables [Unit]	Value
T_M [Nm]	0.20
K [N/m]	15 – 150
D [Ns/m]	0.30 – 2.7

Table 4 : Simulation conditions for enlarging θ_{hop}

Variables [Unit]	Value
$T_{M_{\mathrm{small}}}$ [Nm]	0.0012
$T_{M_{\mathrm{large}}}$ [Nm]	0.20
K [N/m]	15
D [Ns/m]	0.30
$t_{\mathrm{threshold}}$ [s]	1.6 – 2.8

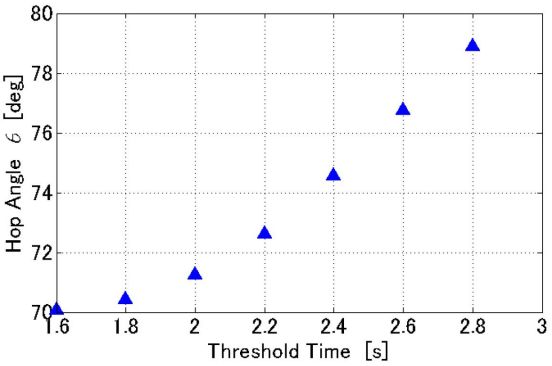

Figure 7: Hop angle against $t_{\text{threshold}}$

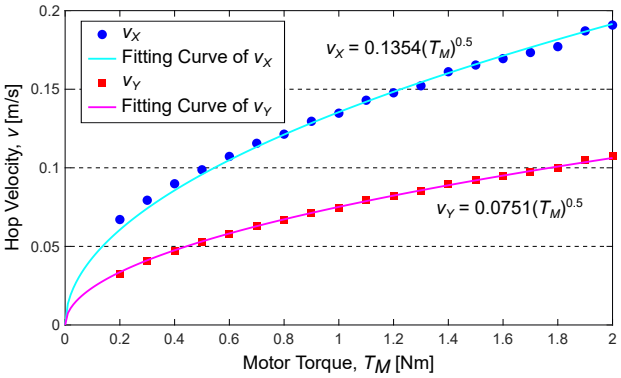

Figure 8: Hop velocity against T_M

the hop angle by utilizing the elastic and damping forces derived from its spikes. By utilizing the forces, when the torque of the motor is small, the robot can gain its horizontal portion of the translational velocity while holding the static friction of its spike in contact with the ground. We conduct some simulations to analyze the hop angle in this case by applying a small torque to the robot for a certain period (threshold time $t_{\text{threshold}}$) and then applying a large enough torque to hop. The torque and threshold time used in this simulation are listed in Tab. 4.

Fig. 7 shows the result of these simulations and plots the hop angle against the threshold time. In Fig. 7, the longer threshold time enlarges the hop angle. When the threshold time is long, the spike can maintain static friction with the ground longer, thus, the robot can obtain a relatively large horizontal component of the translational velocity by the time of transferring to the hopping. If the robot obtains a large horizontal component of the translational velocity, the hop angle ($\theta_{\text{hop}} = \tan^{-1} v_{x_{\text{hop}}}/v_{y_{\text{hop}}}$) increases and the robot can traverse a large distance at each hop.

4.2 Analyses of Hop Velocity

In this section, we evaluate the hop velocity ($v_{x_{\text{hop}}}$, $v_{y_{\text{hop}}}$) of the robot. We assign several values of the torque to the robot over each simulation and observe the behavior of the robot. The conditions of this simulation are listed in Tab. 5. Fig. 8 displays the hop velocity in x and y directions against the torque. In the case of hopping, the relatively large torque is induced, therefore, a spike in contact with the ground slips on the ground and the large torque generates much larger pushing forces than the elastic and damping forces generated by the robot's spikes. Besides, in this case, the elastic and damping forces are irrelevant to the torque if K and D do not change because the shrinkage of the spike depends on the attitude of the robot before detaching from the ground. Moreover, in the case that the robot receives a large torque and hops, the robot rotates pretty fast, therefore, the period of maintaining the contact with the ground becomes too short. For these reasons, in Fig. 8, the elastic and damping forces induced by the external compliances almost do not affect the impulse which the robot receives until starting the hopping motion and v_x and v_y can be affected by the magnitude of the torque. Hence, the impulse which the robot receives until the detachment is approximated as follows:

$$F \propto T_M \tag{8}$$

$$\Delta t \propto \sqrt{\frac{1}{T_M}} \tag{9}$$

$$F\Delta t \propto \sqrt{T_M} \tag{10}$$

From these equations, the hop velocity is approximately proportional to the square root of T_M. In this case, the characteristics of the hop velocity is almost the same as hopping rovers which do not have external compliances (e.g. MINERVA [3]).

Table 5: Simulation conditions for analyzing hop velocity

Variables [Unit]	Value
T_M [Nm]	0.20 – 1.0
K [N/m]	15
D [Ns/m]	0.30

5 ANALYSES OF TUMBLING MOBILITY

We address the tumbling mobility of the proposed mechanical system in this section. Several numerical analyses are conducted to evaluate the characteristics of the tumbling motion. In this simulation, the torque of the motor is applied to the robot over the simulation. Therefore, the proliferation rate of the

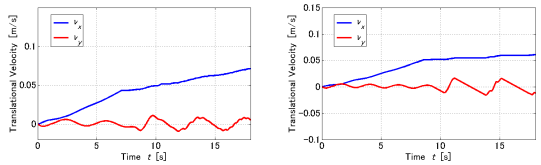

(a) $K = 15$ N/m (b) $K = 30$ N/m

(c) $K = 45$ N/m (d) $K = 60$ N/m

Figure 9: Relationship between K and Translational Velocity while Tumbling

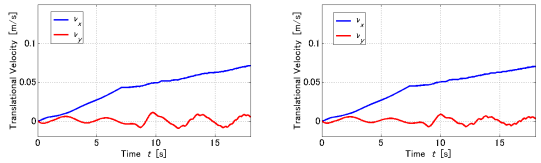

(a) $D = 0.3$ Ns/m (b) $D = 0.9$ Ns/m

(c) $D = 1.5$ Ns/m (d) $D = 2.1$ Ns/m

Figure 10: Relationship between D and Translational Velocity while Tumbling

translational velocity changes as the spikes' state of friction transfers from static to dynamic. The parameter of the robot is listed in the same Tab. 2.

In this section, we analyze the translational velocity of the robot during tumbling locomotion. The torque of the motor is applied to the robot over these simulations. At first, we assign several elastic coefficient K to the spikes and mention the variation of the translational velocity during tumbling locomotion. The conditions for this simulation are listed in Tab. 6. Figure 9 plots the translational velocity against the time at each case. The x portion of the

Table 6: Simulation conditions for analyzing translational velocity assigning various K

Variables [Unit]	Value
T_M [Nm]	0.0050
K [N/m]	15 – 60
D [Ns/m]	0.30

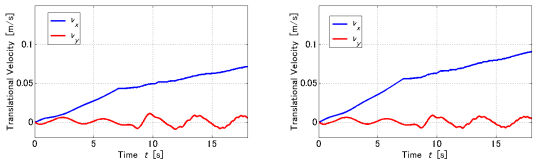

(a) $T = 0.005$ Nm (b) $T = 0.006$ Nm

(c) $T = 0.007$ Nm (d) $T = 0.008$ Nm

(e) $T = 0.009$ Nm (f) $T = 0.01$ Nm

Figure 11: Relationship between Torque and Translational Velocity while Tumbling

translational velocity does not tend to increase with the increment of K. If K is large, it becomes difficult for the robot to maintain its contact with the ground due to the increment of the natural frequency. Moreover, the period of floating becomes longer. Therefore, the x portion of the translational velocity does not increase well when K is large.

Besides, we address the case that the various damping coefficient D are assigned to the spikes. The conditions for this simulation are listed in Tab. 7. Fig. 10 displays the translational velocity against the time at each case. In this case, the translational velocity decreases since the spikes can easily dissipate its reaction forces for propulsion. Finally, we men-

Table 7: Simulation conditions for analyzing translational velocity assigning various D

Variables [Unit]	Value
T_M [Nm]	0.0050
K [N/m]	15
D [Ns/m]	0.30 – 2.1

Table 8: Simulation conditions for analyzing translational velocity assigning various T_M

Variables [Unit]	Value
T_M [Nm]	0.0050 – 0.0010
K [N/m]	15
D [Ns/m]	0.30

tion the case that we assign several torques T_M to the robot. The conditions for this simulation are listed in Tab. 8. Fig. 11 indicates that the translational velocity against the time at each case. In this case, the x component of the translational velocity increases because as described in Eq. 4, the reaction forces of the robot can be affected by T_M.

6 CONCLUSION

In this paper, we evaluated the characteristics of the tumbling and the hopping mobility by numerical simulations. The hop angle is not affected by the elastic and damping coefficient of the spikes and by utilizing the elastic and damping forces of the spikes, we can enlarge the hop angle. The torque of the motor enlarges the hop velocity and the hop velocity is almost proportional to the square root of the torque. On the other hand, the tumbling motion is affected by the elastic coefficient of the spikes and a large elastic coefficient K leads the robot to float. The large torque T_M can also increase the translational velocity during tumbling locomotion.

References

[1] B. H. Wilcox and R. M. Jones, "The MUSES-CN nanorover mission and related technology," in Proc. 2000 IEEE Aerospace Conf., Big Sky, MT, 2000, vol.7, pp. 287-295.

[2] K. Takahashi, S. Shimoda, K. lizuka and T. Kubota, "A study of locomotion mechanism based on gravitational environment," in Proc. 2004 IEEE/RSJ Int. Conf. Intel. Rob. Syst., Sendai, Japan, 2004, pp. 4001-4006.

[3] T. Yoshimitsu, T. Kubota, I. Nakatani, T. Adachi and H. Saito, "Micro-hopping robot for asteroid exploration," Acta Astronaut., 2003, vol.52, pp. 441-446.

[4] L. Witte, J. Biele, A. Braukhane, F. Herrmann, T. -M. Ho, C. Krause, S. Kuß, C. Lange, M. Schlotterer, S. Ulamee, S. Wagenbach, "The Mobile Asteroid Surface Scout (MASCOT) - System & Mission Engineering and Surface Operations Concept," in Proc. Global Space Exploration Conf. 2012, Washington D.C., 2012.

[5] B. Hockman, A. Frick, R. G. Reid, A.D. Nesnas and M. Pavone, "Design, Control, and Experimentation of Internally-Actuated Rovers for the Exploration of Low-gravity Planetary Bodies," J. Field Robot., 2017, vol. 34, pp, 5-24.

[6] K. Nagaoka, K. Watanabe, T. Kaneko and K. Yoshida, "Mobility Performance of Ciliary Locomotion for an Asteroid Exploration Robot under Various Experimental Conditions," in Proc. 13th Int. Symp. Artif. Intel., Robot. and Autom. in Space, Beijing, China, S-5a-2, 2016.

[7] A. Parness, N. Abcouwer, C. Fuller, N. Wiltsie, J. Nash and B. Kennedy, "LEMUR 3: A limbed climbing robot for extreme terrain mobility in space," in Proc. 2017 IEEE Int. Conf. Robot. Autom., Singapore, 2017, pp. 5467-5473.

[8] T. Yoshimitsu, "Development of autonomous rover for asteroid surface exploration," in Proc. 2004 IEEE Int. Conf. Robot. Autom., New Orleans, LA, 2004, pp. 2529-2534.

[9] Y. Tsumaki, T. Akaike, R. Kazama, T. Mineta and R. Tadakuma, "Environment-Driven Rover for Asteroid Exploration," in Proc. 11th Int. Symp. Artif. Intel., Robot. Autom. in Space, Turin, Italy, P-20, 2012.

[10] S. Shimoda, T. Kubota and I. Nakatani, "New mobility system based on elastic energy under microgravity," in Proc. 2002 IEEE Int. Conf. Robot. and Autom., Washington, DC, 2002, pp. 2296-2301.

[11] K. Ioi, "A mobile micro-robot using centrifugal forces," in Proc. 1999 IEEE/ASME Int. Conf. Adv. Intel. Mechatr., Atlanta, GA, 1999, pp. 736-741.

[12] K. Kobashi, A. Bando, K. Nagaoka and K. Yoshida, "Tumbling and Hopping Locomotion Control for a Minor Body Exploration Robot," in Proc. 2020 IEEE/RSJ Int. Conf. Intel. Rob. Syst., Las Vegas, NV, 2020.